J Mater Sci (2019) 54:11526–11537

Electronic materials

Effect of Ti doping on the crystallography, phase, surface/interface structure and optical band gap of Ga_2O_3 thin films

Sandeep Manandhar[1], Anil K. Battu[1], Susheng Tan[2], Rahul Panat[3], V. Shutthanandan[4], and C. V. Ramana[1,*]

[1] Center for Advanced Materials Research (CMR), University of Texas at El Paso, 500 W University Ave., El Paso, Texas 79968, USA
[2] Department of Electrical and Computer Engineering, and Petersen Institute of NanoScience and Engineering, University of Pittsburgh, 3700 O'Hara Street, Pittsburgh, PA 15261, USA
[3] Department of Mechanical Engineering, Carnegie Mellon University, 5000 Forbes Ave., Pittsburgh, PA 15213, USA
[4] Environmental Molecular Sciences Laboratory (EMSL), Pacific Northwest National Laboratory (PNNL), Richland, WA 99352, USA

Received: 19 December 2018
Accepted: 27 April 2019
Published online: 28 May 2019

ABSTRACT

The effect of titanium (Ti) doping on the crystal structure, phase, surface/interface chemistry, microstructure and optical band gap of gallium oxide (Ga_2O_3) (GTO) films is reported. The Ti content was varied from 0 to ~ 5 at% in co-sputtering, using Ga_2O_3 ceramic and Ti metal targets, deposited GTO films produced. The sputtering power to the Ti target was varied in the range of 0–100 W, while keeping the sputtering power to Ga_2O_3 constant at 100 W, to produce GTO films with 0–5 at% Ti. The Ti-incorporation-induced effects were significant for the crystal structure, phase, surface/interface chemistry and morphology, which in turn induce changes in the band gap. The high-resolution core-level X-ray photoelectron spectroscopy (XPS) analyses confirm that the Ga ions exist as Ga^{3+} in both intrinsic Ga oxide and GTO films. However, XPS data reveal the formation of Ga_2O_3–TiO_2 films with the presence of Ti^{4+} ions with increasing Ti sputtering power, i.e., higher Ti contents in GTO. Evidence for the formation of nanocrystalline Ga_2O_3–TiO_2 films was also found in the structural analyses performed using electron microscopy and grazing incidence X-ray diffraction. Significant band gap reduction (E_g ~ 0.9 eV) occurs in GTO films with increasing Ti dopant concentration from 0 to 5 at%. A correlation between the Ti dopant concentration, surface/interface chemistry, microstructure and band gap of GTO films is established.

Address correspondence to E-mail: rvchintalapalle@utep.edu

https://doi.org/10.1007/s10853-019-03663-w

Introduction

Gallium oxide, one among the wide band gap oxides, is an interesting material for many of the current and emerging technological applications [1–20]. β-Ga_2O_3 has emerged as a promising candidate for sensors [1–3], memory devices [4] and solar-blind deep UV detectors [5, 6]. The future prospects in power electronics, UV-based devices and luminescent displays generate renewed interest in β-Ga_2O_3 [10–13]. Current interest in intrinsic and hybrid materials of Ga_2O_3 is directed toward tailoring the functionality by manipulating the architectures and morphology at the nanoscale dimensions to meet the enhanced device performance [2, 6–14].

Gallium-oxide-based single-phase as well as multicomponent architectures or hybrid materials with nanostructured morphologies continue to attract the scientific and research community in view of their fascinating properties and emerging technological applications. In this context, it is important to recognize that the applications involving intrinsic and doped/hybrid Ga_2O_3-based materials are continuously evolving [18]. One particular aspect of these contemporary studies is doping or hybridizing Ga_2O_3 to derive new properties and phenomena, which can facilitate designing materials for energy-related applications [9, 18]. For instance, recently demonstrated enhanced performance of Ga_2O_3–graphene oxide hybrid nanomaterials suggests the possibility to design new electrode materials for lithium ion batteries [18]. Selecting or designing material systems by combining all the advantages of each material component is considered as an ingenious approach to design efficient materials for high-performance electrochemical energy storage and conversion devices [19–25]. While rechargeable Li-ion batteries represent one of the most attractive technologies for advanced electrochemical energy storage, the development of new anode and cathode materials with higher capacity is critical for meeting the future portable energy needs [9, 18, 21]. Recent reports on utilizing Ga-oxide-based nanomaterials demonstrate that the lithiation behavior in such materials is worthy of further detailed research activities on both intrinsic and doped Ga oxides, which may lead to a new avenue for the exploration of long-life and high-capacity anode materials for LIBs [9, 18]. Carefully engineered ceramic composites combined with graphene sheets caused extrinsic defects and more active sites; both increased the lithiation and anode stability [21]. Such recently discovered new phenomena assure the possibility of the design and development of novel electrode materials based on Ga oxide and its composites.

It is well known that the properties and device applications of β-Ga_2O_3 can be tuned or controlled by doping with carefully chosen metal ions [2, 7, 15–18]. In fact, several research groups have paid attention to tune their structural, chemical, physical, mechanical, optical and electrical properties by various means, such as elemental/ion doping, adopting different chemical/physical synthetic routes, fabricating thin films using chemical and physical deposition methods. Specifically, in order to further improve the functionality and performance of Ga_2O_3, doping using either isovalent and/or multivalent ion(s) has been considered in the literature [2, 7, 15–18]. For instance, doping of β-Ga_2O_3 with Sn, Cr, Ti, Mo or W induces changes in the optical properties [2, 7, 15–18]. We recently reported the structure–band gap relation in Ti-doped Ga_2O_3 films in a communication [15]. However, a more detailed account of fundamental understanding of the Ti chemistry, overall chemical composition, crystal structure, phase, morphology, microstructure and optical properties is quite important to establish a structure–property correlation, which can serve as a road map for practical utilization of Ti-doped Ga_2O_3 films. To accomplish this scientific objective, in this work, a detailed investigation is carried out, while the results are presented and discussed in this paper.

Experimental

Fabrication

Ti-doped Ga_2O_3 (GTO) films were deposited onto silicon (Si) (100) substrates, which were systematically cleaned by ultrasonication using ethyl alcohol and dried with nitrogen. Ga_2O_3 (99.999%) and Ti (99.95%) targets (2 in. diameter; Plasmaterials Inc.) were co-sputtered to synthesize GTO films [15]. The deposition chamber base pressure was better than $\sim 10^{-6}$ Torr. During deposition, Ga_2O_3 target was kept at a constant sputtering power of 100 W, while that of Ti target was varied from 0 to 100 W to produce GTO films with variable Ti concentrations. All the depositions were taken by a substrate

temperature (T_s) of 500 °C, which results in nanocrystalline β-phase Ga_2O_3 films [16, 17]. The deposition was taken for a constant time of 3 h; however, this resulted in film thickness increase continuously from 190 to 290 nm, which is primarily due to variable sputtering powers to the Ti target. For clarity and understanding the results, the GTO sample identification numbers were generated using the sputtering power applied to the Ti target.

Characterization

The Rutherford backscattering spectrometry (RBS) measurements were taken with 1.5 MeV He^+ ions using ion accelerator (3 MeV NEC Tandem Ion Accelerator). The backscattered helium ions were collected at the scattering angle of 160° using a surface barrier detector. SIMNRA simulation software was used for calculations and simulating the experimental RBS data/spectra [26]. These calculations yield the chemical composition and thickness [17, 26]. The detailed procedure on using this simulation to obtain the stoichiometry and atomic concentration in the films has been outlined elsewhere [17]. In the calculations, the following set of experimental parameters were kept constant: incident energy, integrated charge, detector resolution (energy), and scattering geometry [17, 26].

Kratos AXIS Ultra DLD spectrometer was used for XPS measurements. Al Kα monochromatic X-ray source (1486.6 eV) and a high-resolution hemispherical analyzer were used. Measurements were taken following a detailed, systematic procedure established for both intrinsic and doped Ga oxides [2, 17]. The binding energy (BE) of carbon (C 1 s) at 284.8 eV was used as the charge reference. Survey scans were typically carried out at pass energies of 80 or 160 eV, while high-resolution scans were performed at a pass energy of 20 eV. The error of estimation is ± 0.01 at% for Ga, Ti and O atomic concentration reported.

AFM images (512 scan lines and 512 pixels per scan line) were acquired with an integral gain of approximately 2, a proportional gain of approximately 50 and an amplitude set point of 300 mV. The drive amplitude varied between 30 and 180 mV. The images were then subjected to a third-order flattening procedure using the Veeco Nanoscope software to remove the nonlinear background artifact introduced by the piezo scanner. The surface roughness was quantified over five areas of 1 μm × 1 μm on the 5 μm × 5 μm scan size images.

Crystal structure and phase analysis of the Ga_2O_3 films deposited under variable Ti sputtering powers were analyzed using X-ray diffraction (XRD) and transmission electron microscopy (TEM) measurements. Grazing incidence X-ray diffraction (GIXRD) measurements on Ga_2O_3 films deposited on Si were performed using a Bruker D8 Advance X-ray diffractometer. All the measurements were taken ex situ as a function of Ti content. GIXRD patterns were recorded using CuKα radiation (λ = 1.54056 Å) at room temperature. For TEM, the GTO films were characterized using a Thermo Fisher Scientific (formerly FEI) Titan Themis G2 200 probe Cs-corrected scanning transmission electron microscope (STEM) in TEM mode operated at 200 keV. The morphology and selective area diffraction (SAED) of the films were recorded with a Ceta CMOS camera. The specimen for TEM observation was prepared using an FEI Scios focused ion beam (FIB)/scanning electron microscope (SEM) dual-beam system following the established procedure for TEM specimen preparation. First, a thin carbon film of 15 μm × 2 μm × 0.5 μm and then a Pt film of 15 μm × 2 μm × 2 μm were deposited on the Ga_2O_3 sample using electron beam and focused ion beam, respectively, to protect the sample surface from ion damaging during milling; then, the surrounding materials around the protected region were milled away using 30-kV high-current ion beam; after initial cleaning and cutting, the specimen lamellae were transferred to Cu TEM grid; the lamellae were further thinned to < 100 nm and further cleaned using 5-kV and 2-kV low-current ion beam, respectively. The final lamellae were electron transparent about 60–80 nm and characterized using TEM.

Results and discussion

Chemical composition

Figure 1 shows the RBS data of GTO films; the arrows indicate the energy position of the backscattered ions from respective atoms present in GTO–Si configuration. Ga peak is located at higher energy (~ 1140 keV) because it is the heaviest among the constituent atoms/elements in the entire GTO-Si(100) assembly. The step edge and peaks due to ion

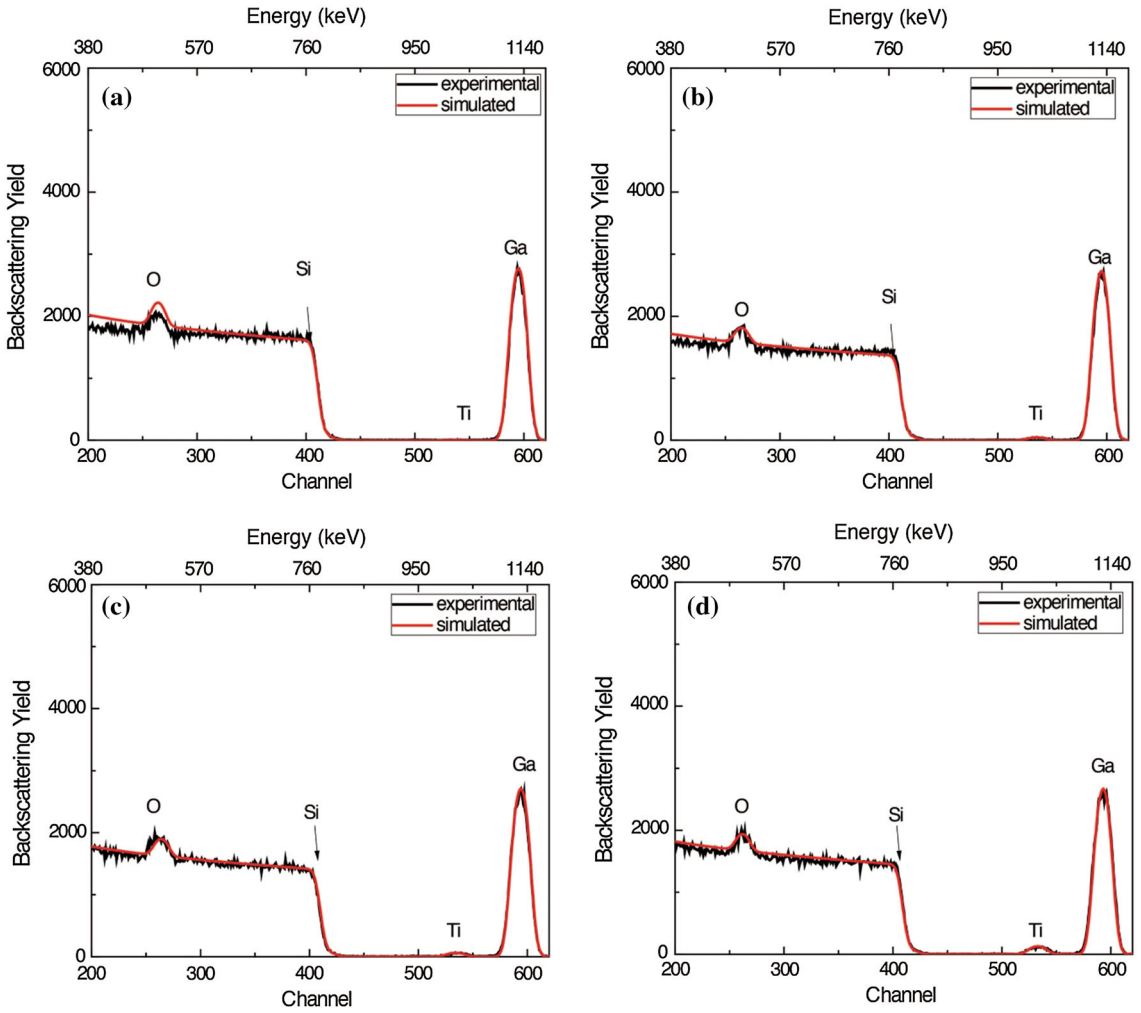

Figure 1 RBS data of Ga–Ti–O films deposited with variable Ti contents. The data shown are for: **a** intrinsic Ga_2O_3; **b** GTO-60; **c** GTO-80; and **d** GTO-100. Data shown include experimental curves (circles) and SIMRA simulated curves (lines). The backscattered ions due to Ga, Ti, Si and O and their respective energy positions are as indicated. A reasonable agreement between the experimental and simulated RBS curves can be seen.

backscattering from Si (substrate) and O atoms (film) are observed at ~ 810 and 270 keV, respectively (Fig. 1). No evidence of backscattered ions due to Ti is seen in the RBS data of intrinsic Ga oxide films. The evolution of Ti peak (~ 1030 keV) is clearly seen in the RBS spectra as the sputtering power applied to the Ti target increases. The Ti or Ga peaks are related to the atomic concentration and thickness distribution of respective atoms in the GTO film. It can be seen in Fig. 1 that the simulated data are in reasonable agreement with the experimental data. Thus, for GTO-0 films, i.e., without any Ti, the RBS data indicate Ga:40 at% and O:60 at% leading to O/Ga ratio of 1.5, which is expected theoretically. The Ti content estimated from RBS data is shown in Fig. 2. For clarity purposes, the evolution of Ti peak with sputtering power is presented in the inset of Fig. 2. Increasing Ti content from 0 to ~ 5 at% is evident with increasing sputtering power from 0 to 100 W. Furthermore, the Ti concentration was also calculated from the XPS spectral intensity of Ti 2p, as appear in subsequent discussion, where a steady increase in Ti content from 0 to 5 at% was noted. Thus, combined RBS and XPS measurements and reasonable agreement of the results in both studies confirm the chemical homogeneity and also allows to translate the Ti sputtering power into Ti atomic concentration, which is varied from 0 to 5 at% in the GTO films.

XPS measurements allowed us to understand the chemical valence states of constituent ions in addition

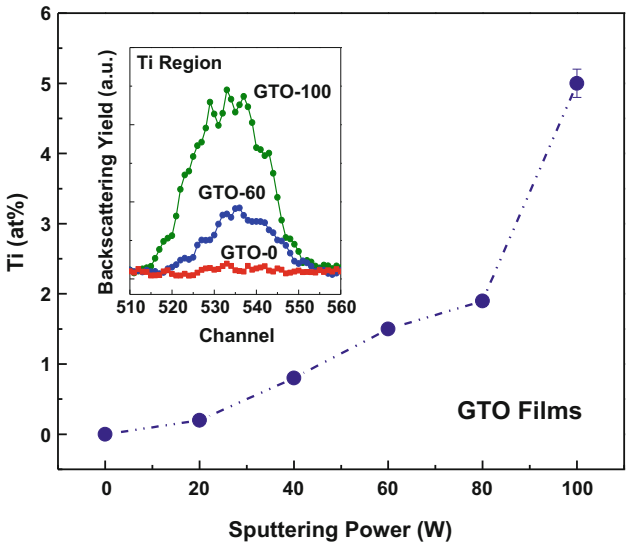

Figure 2 Ti concentration with sputtering power. It is evident that the Ti content increases from 0 to ~ 5 at% with increasing sputtering power from 0 to 100 W.

to the surface chemical composition of GTO films. The core-level XPS spectra of the Ga 3d region for GTO samples (Fig. 3a). Ga 3d peak is located at a binding energy (BE) of ~ 20.5 eV, which agrees to the literature [27, 28]. Figure 3b shows the high-resolution core-level XPS of O 1 s. The O 1 s peak for GTO-0 (intrinsic Ga_2O_3) is located at BE ~ 530.8 eV, which is consistent with the values reported in the literature [29, 30]. This BE is usually assigned to oxide (Ga–O–Ga bonds), which corresponds to the position of O 1 s for Ga_2O_3 when gallium is present in Ga^{3+} chemical state [31–33]. For O 1 s, the shoulder at higher BE side is generally related to O bonded to C (labeled as CO_2). However, increasing Ti content in GTO films results in a slight shift in the BE position of O 1 s peak due to increasing Ti–O bonds in GTO. The peak at 530.3 eV of BE relates to Ti_2O_3 [34–36]. Thus, Ti occupies Ga sites in gallium oxide structure. The XPS data of Ti 2p (Fig. 3c) provide evidence for the Ga_2O_3–TiO_2 composite formation (for higher Ti contents). For Ti $2p_{3/2}$, BE of 458.6 eV and 457.13 eV to Ti^{4+} (TiO_2) and Ti^{3+}(Ti_2O_3), respectively [37–39]. Ti^{4+} does not have unpaired d electrons and does not exhibit multiplet splitting, but Ti^{3+} has unpaired d electrons and theoretically exhibits multiplet structure which may not be well resolved [40]. It can be seen that, for GTO-100 samples, XPS data indicate predominantly TiO_2 confirming the formation of Ga_2O_3–TiO_2 composite, which is further evidenced in TEM analyses.

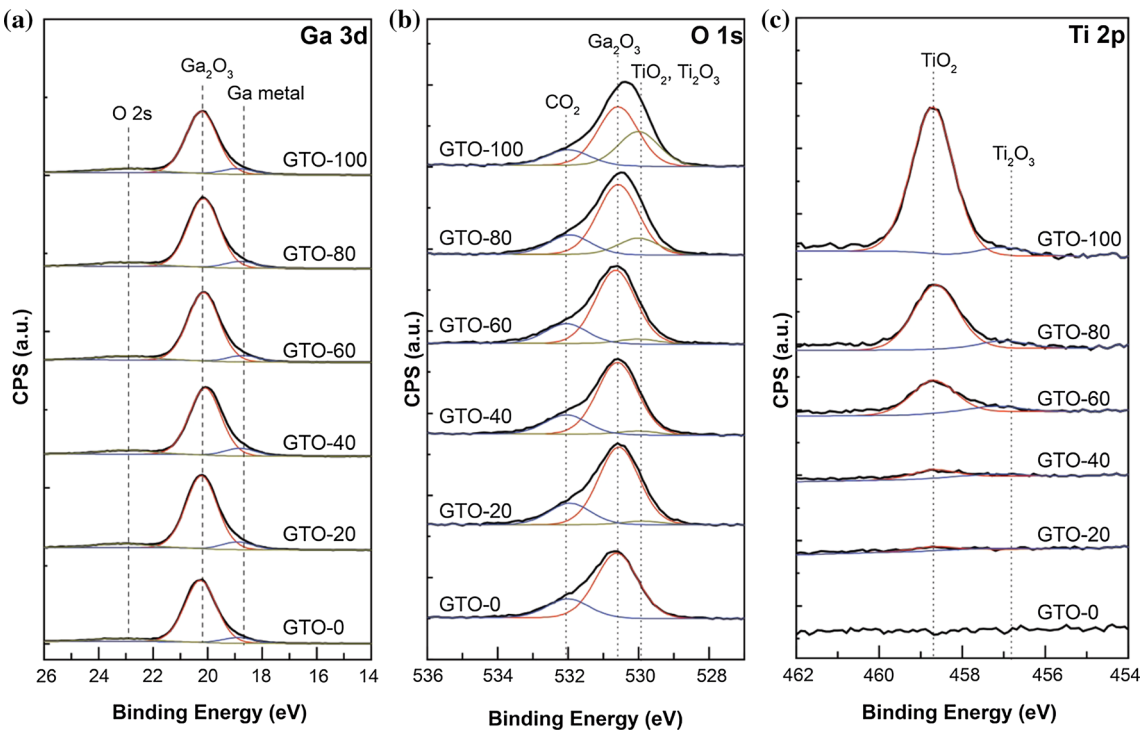

Figure 3 High-resolution XPS data of Ga, O, and Ti core-level peaks in GTO films deposited with variable Ti concentrations. **a** Ga 3d high-resolution XPS spectra. **b** O 1 s high-resolution XPS spectra. **c** Ti 2p core-level XPS spectra.

Surface morphology—atomic force microscopy (AFM)

The AFM data of GTO films are shown in Fig. 4. The topographic images along with the corresponding 3D surface images are shown. For GTO-0 films, i.e., without Ti, nanoparticulate morphology of the film surfaces, where the conically shaped grains are distributed uniformly all over the film surface, is evident. The root-mean-square surface roughness value noted for intrinsic Ga_2O_3 films was $\sim$ 1 nm. The AFM results of intrinsic Ga_2O_3 films are in excellent agreement with those reported in the literature [31, 41]. The remarkable effect of Ti doping on the surface morphology of Ga_2O_3 films is evident in the AFM data of samples deposited with increasing sputtering power of Ti from 40 to 100 W. While the effect is not pronounced in the beginning, the effect of Ti is reflected in terms of size reduction and making film surfaces smoother as evident in the AFM data. The effect is more visible for GTO-100 samples, which are deposited with the highest sputtering power to the Ti target. Thus, the Ti content in Ga_2O_3 films retains the well-resolved uniform morphology and densely packed grains and grain boundaries until 1 at%, at which point changes become significant. Such changes in surface morphology were also evident in W-doped Ga_2O_3 films. In addition, Ti-incorporation-induced disordering and surface amorphization were reported in Ti-doped WO_3 films [42, 43]. Thus, when the AFM results are considered along with XPS surface chemical analysis, it is clear that the Ti-doping-induced formation of Ga_2O_3–TiO_2 composite is the origin of observed morphology trend noted with Ti doping.

Crystal structure and phase

The GIXRD patterns of GTO samples are presented in Fig. 5. The XRD patterns of GTO-0, i.e., without any Ti, indicate the formation of nanocrystalline β-Ga_2O_3. The diffraction peaks correspond to the monoclinic β-phase (space group C2/m) with the observed peaks: ($\bar{2}$01), (400), (002) (111), (510), and ($\bar{2}$04) at 2θ values of 18.95, 30.05, 31.74, 35.17, 48.59, and 64.17, respectively [44]. The indexing of the peaks is performed according to JCPDS (00-043-1012). The evolution of these peaks shows an interesting trend as a function of Ti incorporation into Ga_2O_3 nanocrystalline films. The very first characteristic feature that can be noted is the dominance of the (400) peak at 2θ = 30.05° for intrinsic Ga_2O_3 nanocrystalline films (Fig. 5). The intensity of this peak is seen to increase with Ti incorporation up to 1.5 at%. Coupled with the (400) peak, a slight increase in (111) peak is observed in the XRD patterns. However, changes in the (111) peak are minor compared with the (400) peak. Further increase in the sputtering power to the Ti target beyond 60 W, i.e., Ti content higher than 1.5 at%, seems to introduce structural changes in Ga_2O_3, as is evident from the GIXRD patterns shown in Fig. 5. Clearly, Ti incorporation causes the (111) peak to grow in intensity while suppressing the intensity of the (400) peak. Finally, the (400) and (111) peaks become broader and merge for samples deposited with the highest, equal sputtering powers (100 W) to the Ga_2O_3 and Ti targets. This observation indicates the size reduction and finally amorphization. Chemical analyses (not shown) indicate that the samples with higher Ti contents (> 4 at%) are Ga_2O_3–TiO_2 mixed or composite oxide films instead of single-phase β-Ga_2O_3.

Finally, to better understand the structure evolution with Ti-doping and validate the single phase versus of Ga_2O_3–TiO_2 composite formation as evident in chemical analyses, the local microstructure of the GTO films is probed using TEM measurements as a function of Ti content. The TEM data of intrinsic Ga_2O_3 (GTO-0) films are presented in Fig. 6. TEM image of a thin cross-sectional lamella from GTO-0 film is shown in Fig. 6a, where cross section of the Ga_2O_3 film sample highlights the apparent interfaces between the Si substrate, the Ga_2O_3 film and the C/Pt protective layers. It is evident that the microstructure the Ga_2O_3 films is uniform. The interface microstructure characterizes the dense, columnar structure vertically, while some degree of surface roughness (the waviness) exists along the horizontal direction. The later may be due to disorder on the surface of the film, while the observed interface structure is a characteristic feature of samples performed by sputter deposition and thermodynamic

Figure 4 AFM surface morphology for GTO films. Topographical 2D images (left column) and the corresponding 3D surface images (right column) are shown. All the images are obtained at 500 nm × 500 nm. For clarity purpose, the scale bar is manually added to the 3D image as indicated for one of the images. ▶

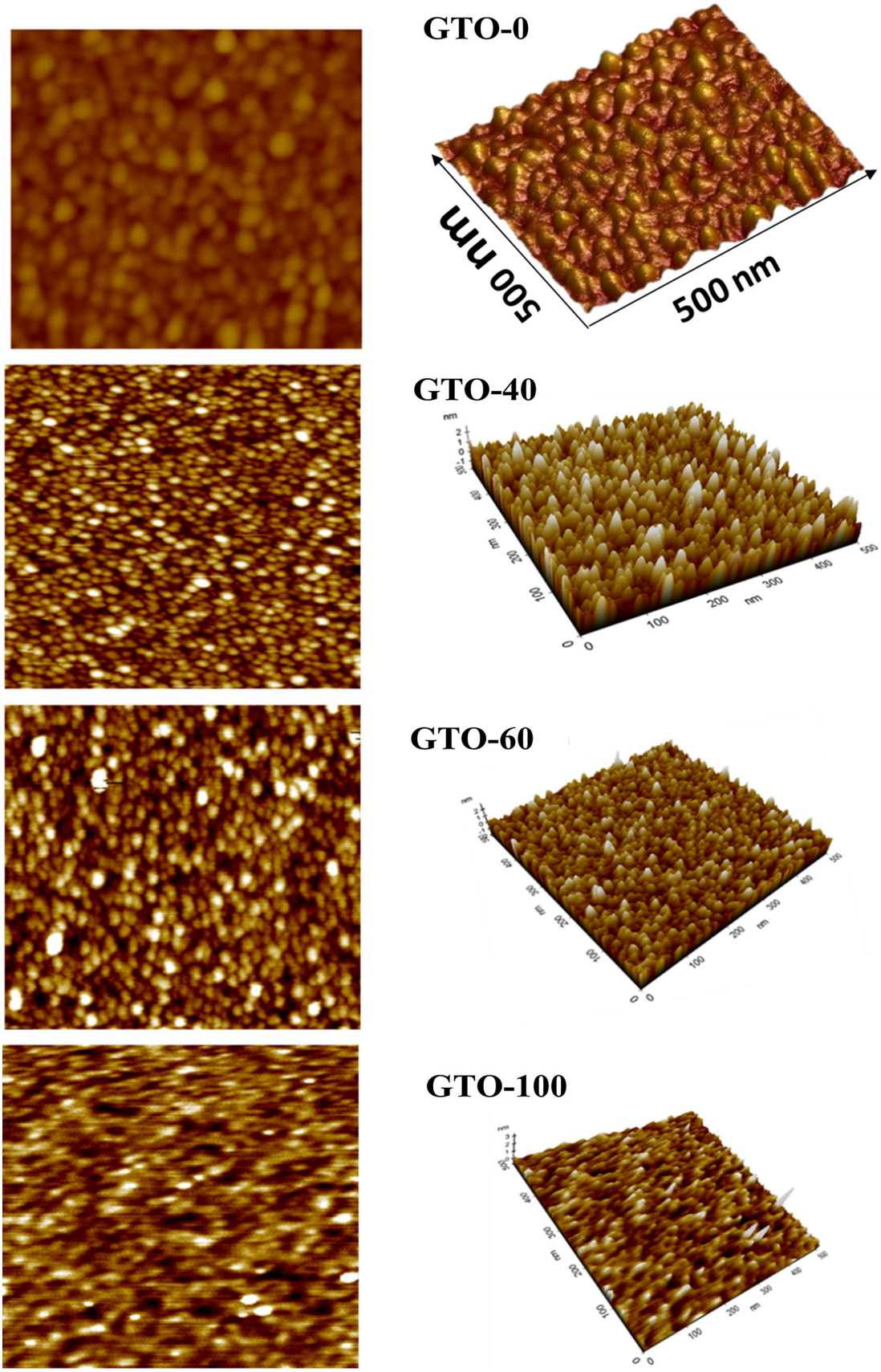
GTO-0
500 nm
500 nm
GTO-40
GTO-60
GTO-100

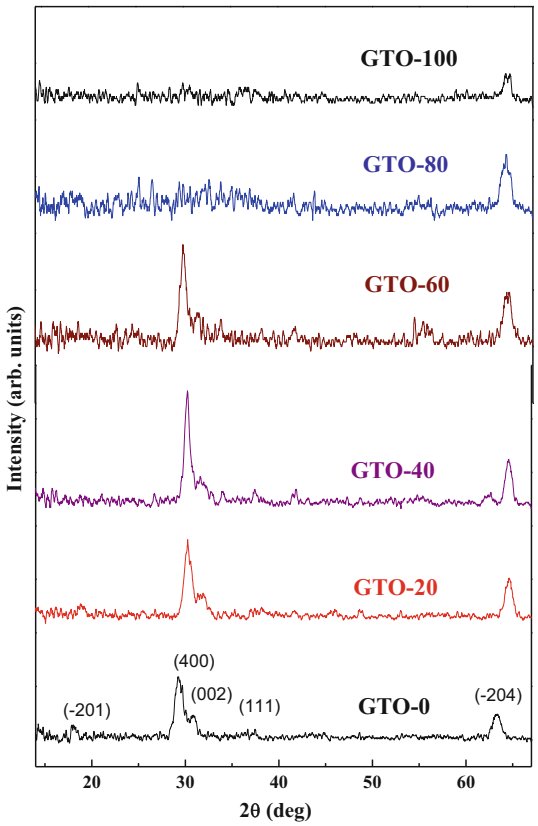

Figure 5 X-ray diffraction patterns GTO films. Structural evolution with increasing Ti content is evident in the patterns. The very first intense peak fully disappears, along with the diffuse nature of the patterns, from GTO films deposited with a sputtering power applied to the Ti target ≥ 80 W.

conditions employed for sample fabrication. The selected area electron diffraction (SAED) patterns of GTO samples are shown in Fig. 6b. It is evident that the SAED pattern exhibits a ring made up of bright spots that indicate that the films were composed of randomly oriented nanocrystalline Ga_2O_3 [44–46]. The pattern was successfully indexed with ICDD PDF4 + database software, and they match with the simulated diffraction patterns of Ga_2O_3. Thus, together with GIXRD analyses, the SAED analyses confirm the formation of nanocrystalline Ga_2O_3 films.

The TEM data of Ti-doped Ga_2O_3 films are shown in Fig. 7. TEM images of a thin cross-sectional lamella from GTO films are shown along with their respective SAED patterns. The cross-sectional lamella from all the GTO films exhibits the interface microstructure similar to intrinsic Ga_2O_3 films. This observation indicates that the Ti incorporation retains the characteristic columnar growth and dense interface microstructure of the Ga_2O_3 films. However, the effect of Ti doping is visible in SAED patterns, which could not be successfully indexed to single-phase Ga_2O_3 films as discussed for GTO-0 films. Instead, the formation of Ga_2O_3–TiO_2 composite occurs with increasing Ti content. While the changes not significant or visible in electron diffraction for GTO-40, the SAED patterns indexed with a high confidence to Ga_2O_3–TiO_2 composite for the samples GTO-60 to GTO-100. The TEM results corroborate with the XPS data, where the formation of Ga_2O_3–TiO_2 composite films with the presence of increasing Ti^{4+} ions with increasing sputtering power to the Ti target was evident. Additionally, as reported in detail elsewhere [15, 46], the GIXRD data also indicate the formation of single-phase, nanocrystalline β-Ga_2O_3 for intrinsic and relatively low Ti-doping concentration. However, XRD showed a remarkable trend with Ti doping into Ga_2O_3 where peak broadening and merging

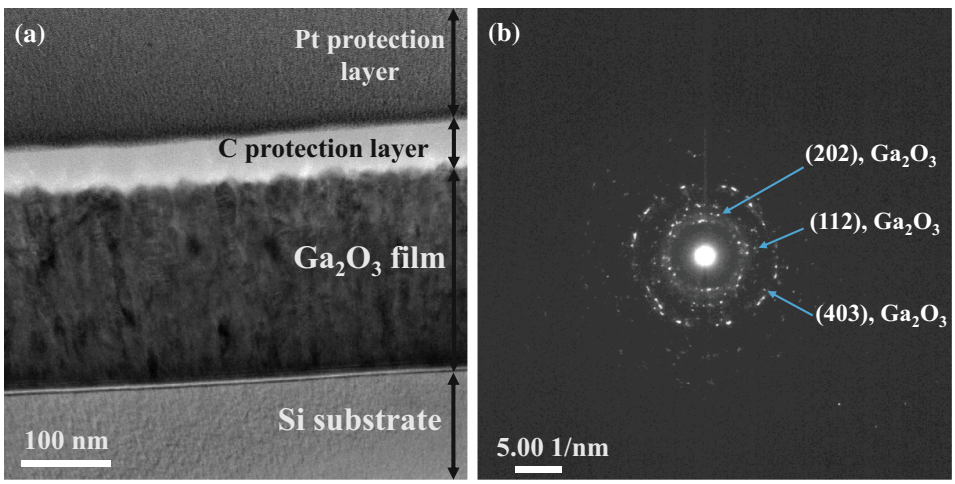

Figure 6 TEM data of intrinsic Ga_2O_3 films. **a** TEM image of a thin cross-sectional lamella from GTO-0 film; **b** SAED pattern of Ga_2O_3 films. The presence of rings made up of bright spots indicates that the films were composed of randomly oriented nanocrystalline Ga_2O_3.

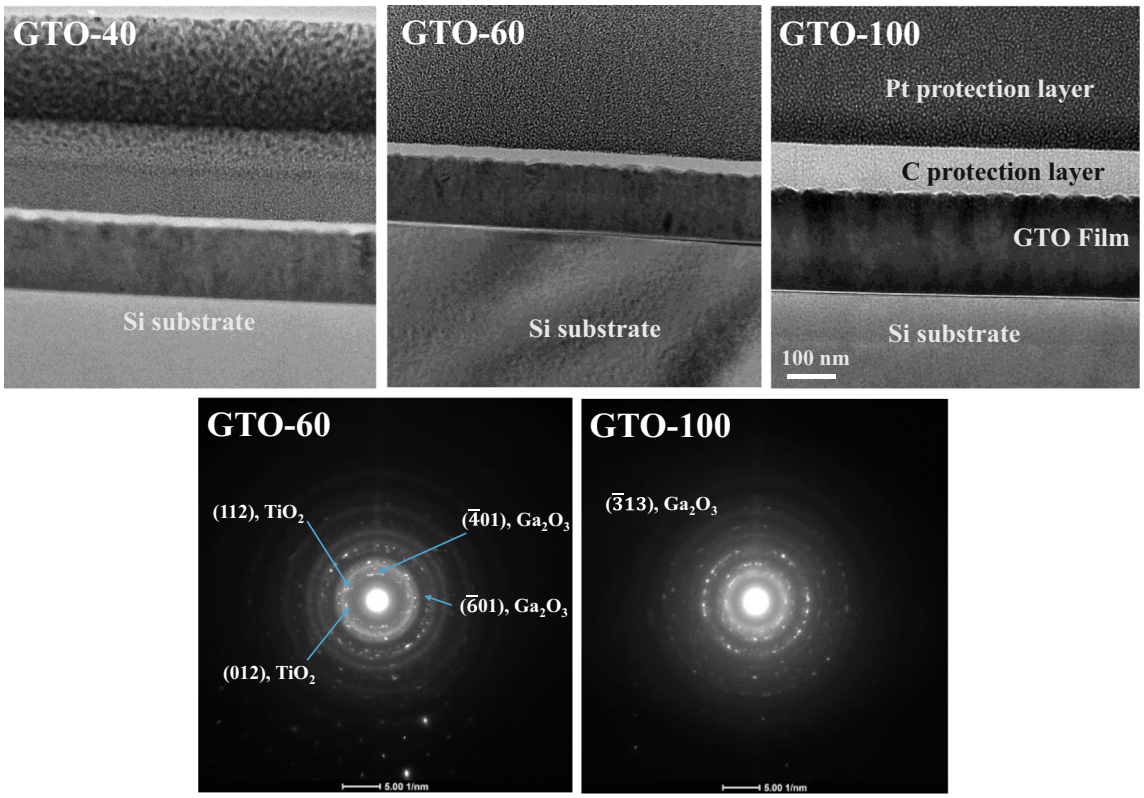

Figure 7 TEM data of GTO films. The TEM images of a thin cross-sectional lamella from GTO films as a function of increasing Ti content are shown (top panel). The corresponding SAED patterns of GTO films are also presented (bottom panel). Emergence of complex ring pattern, compared to intrinsic Ga_2O_3, is evident in Ti-doped Ga_2O_3.

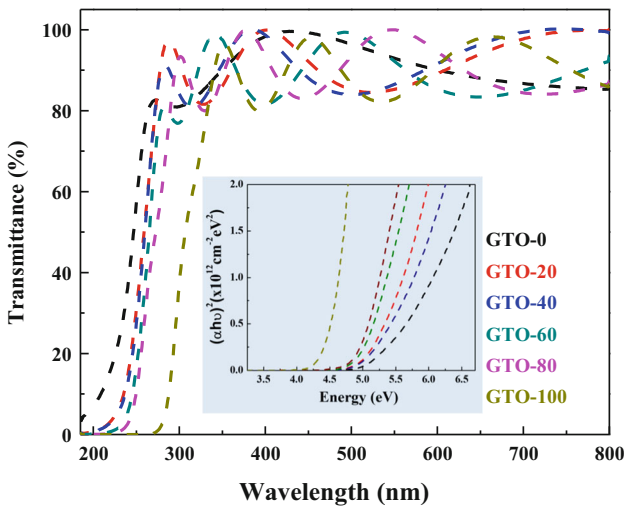

Figure 8 Spectral transmittance characteristic of GTO films. A marked shift in the absorption edge with increasing sputtering power to the Ti metal target is evident in the spectral characteristics. The $(\alpha h\nu)^2$ versus $h\nu$ plots for Ga_2–O_3 and Ti-incorporated Ga_2O_3 films are shown in the inset. Extrapolating the linear region of the plot to $h\nu = 0$ provides the band gap value. The optical absorption data indicate a clear, progressive shift in the edge and E_g with increasing Ti content in GTO films.

occurs which is believed to be due to Ga_2O_3–TiO_2 formation.

Optical band gap and structure–composition–optical property correlation

The optical data of GTO films are shown in Fig. 8. Generally, high optical transparency is seen for all the GTO films. The optical spectra were analyzed using the standard procedure [3, 16, 17] for determining the optical absorption coefficient 'α' and evaluating the band gap 'E_g.' The data analysis was performed to understand the effect of Ti incorporation on E_g and to derive a quantitative structure–chemical composition–optical property relationship. The absorption data and the plots obtained for GTO films are shown in inset of Fig. 8. The E_g value for intrinsic Ga_2O_3 (without Ti incorporation) determined from absorption data is 5.40 (± 0.03) eV. The calculated E_g values were found to decrease with increasing sputtering power to the Ti target, i.e., Ti content in the GTO films.

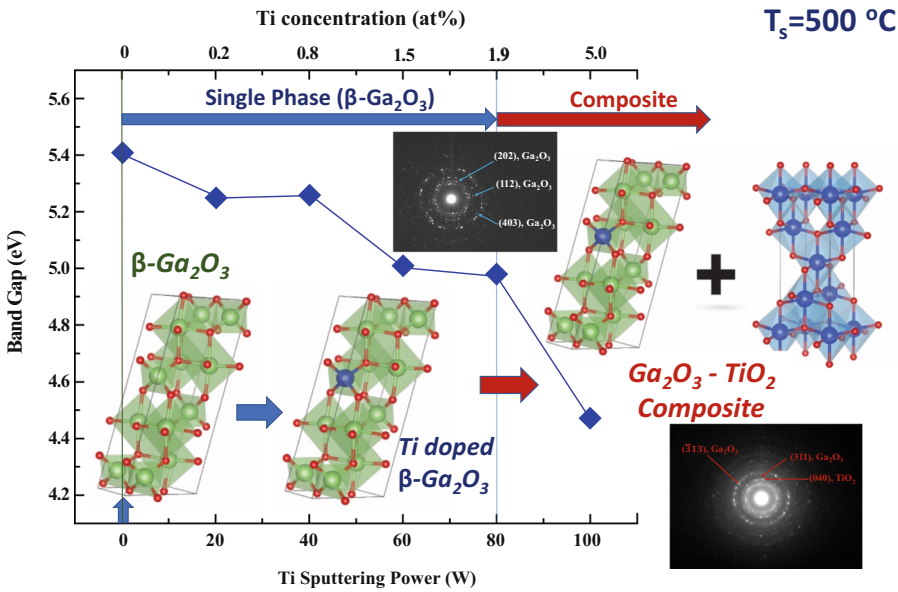

Figure 9 Variation in band gap of GTO films as function of Ti sputtering power. The linked top *X* axis shows the Ti at% determined from chemical analyses. A direct correlation between E_g, Ti content and phase formation is evident.

The variation of E_g of the GTO films is presented in Fig. 9, which also schematically presents the structure–composition–band gap correlation in GTO films. The trend noted in Fig. 9 can be used to explain the effect of Ti incorporation on the structure and band gap of Ga_2O_3. To correlate the optical property changes to Ti content, the Ti concentration (at%) determined from chemical analysis is linked (top *X* axis) to the sputtering power. It is evident that the E_g value decreases continuously with progressive incorporation of Ti in the GTO films. For the highest sputtering power to the Ti target of 100 W, E_g decreases significantly, to 4.47 (± 0.02) eV. The shift in the band gap is ΔE_g = 0.9 eV, which is a quite substantial red shift in the band gap of Ga_2O_3 with Ti incorporation. As evident from structural characterization, increasing Ti concentration leads to single-phase β-Ga_2O_3 to Ga_2O_3–TiO_2 composite formation, which accounts for the observed E_g variation with Ti-content.

Conclusions

The effect of Ti doping on the crystal structure, surface chemistry, and microstructure of Ga_2O_3 films is investigated in detail. The Ti content, which was varied from 0 to ~ 5 at%, significantly influences the crystal structure and phase. While the GTO films exhibit the thermodynamically stable and single-phase β-Ga_2O_3 for lower Ti contents, structural transformation from crystalline to nearly amorphous state occurs with increasing Ti. Higher end of Ti content (~ 5 at%) results in the formation of Ga_2O_3–TiO_2 composite, where the amorphization of the Ga-Ti–O films is attributed to TiO_2 generation. The Ti-incorporation-induced band gap reduction is evident in spectrophotometric analysis. The Ga_2O_3–TiO_2 composite formation for higher Ti contents successfully explains the observed band gap reduction. Structure–composition–band gap correlation established may be useful and provides a road map to produce GTO materials with desirable properties.

Acknowledgements

The authors acknowledge, with pleasure, the support from the National Science Foundation (NSF) with Grant No. ECCS-1509653. CVR also acknowledges the NSF-PREM Grant #DMR-1827745.

References

[1] Pearton SJ, Yang J, Cary PH, Ren F, Kim J, Tadjer MJ, Mastro MA (2018) A review of Ga_2O_3 materials, processing, and devices. Appl Phys Rev 5:011301

[2] Rubio EJ, Mates TE, Manandhar S, Nandasiri M, Shutthanandan V, Ramana CV (2016) Tungsten incorporation into gallium oxide: crystal structure, surface and interface chemistry, thermal stability, and interdiffusion. J Phys Chem C 120:26720–26735

[3] Rubio EJ, Ramana CV (2013) Tungsten-incorporation induced red-shift in the bandgap of gallium oxide thin films. Appl Phys Lett 102:19193

[4] Ogita M, Higo K, Nakanishi Y, Hatanaka Y (2001) Ga_2O_3 thin film for oxygen sensor at high temperature. Appl Surf Sci 175–176:721–725

[5] Fleischer M, Höllbauer L, Meixner H (1994) Effect of the sensor structure on the stability of Ga_2O_3 sensors for reducing gases. Sens Actuators B 18:119–124

[6] Guo D, An Y, Cui W, Cui W, Zhi Y, Zhao X, Lei M, Li L, Li P, Wu Z, Tang W (2016) Epitaxial growth and magnetic properties of ultraviolet transparent $Ga_2O_3/(Ga_{1-x}Fe_x)_2O_3$ multilayer thin films. Sci Rep 6:25166

[7] Guo D, Li P, Wu Z, Cui W, Zhao X, Lei M, Li L, Tang W (2016) Inhibition of unintentional extra carriers by Mn valence change for high insulating devices. Sci Rep 6:24190

[8] Suzuki R, Nakagomi S, Kokubun Y, Arai N, Ohira S (2009) Enhancement of responsivity in solar-blind β-Ga_2O_3 photodiodes with a Au Schottky contact fabricated on single crystal substrates by annealing. Appl Phys Lett 94:222102–222103

[9] Patil SB, Kim IY, Gunjakar JL, Oh SM, Eom T, Kim H, Hwang SJ (2015) Phase tuning of nanostructured gallium oxide via hybridization with reduced graphene oxide for superior anode performance in li-ion battery: an experimental and theoretical study. ACS Appl Mater Interfaces 7:18679–18688

[10] Qian L-X, Wu Z-H, Zhang Y-Y, Lai PT, Liu X-Z, Li Y-R (2017) Ultrahigh-responsivity, rapid-recovery, solar-blind photodetector based on highly nonstoichiometric amorphous gallium oxide. ACS Photonics 4:2203–2211

[11] López I, Lorenz K, Nogales E, Méndez B, Piqueras J, Alves E, García JA (2014) Study of the relationship between crystal structure and luminescence in rare-earth-implanted Ga_2O_3 nanowires during annealing treatments. J Mater Sci 49:1279–1285. https://doi.org/10.1007/s10853-013-7811-x

[12] Higashiwa M, Sasaki K, Kuramata A, Masui T, Amakoshi SY (2014) Development of gallium oxide power devices. Phys Status Solidi A 211:21–26

[13] López I, Nogales E, Méndez B, Piqueras J, Peche A, Ramirez-Castellanos J, Gonzalez-Calet JM (2013) Influence of Sn and Cr doping on morphology and luminescence of thermally grown Ga_2O_3 nanowires. J Phys Chem C 117:3036–3045

[14] Dakhel AA (2012) Structural, optical, and opto-dielectric properties of W-doped Ga2O3 thin films. J Mater Sci 47:3034–3039. https://doi.org/10.1007/s10853-011-6134-z

[15] Manandhar S, Ramana CV (2017) Direct, functional relationship between structural and optical properties in titanium-incorporated gallium oxide nanocrystalline thin films. Appl Phys Lett 110:061902

[16] Battu AK, Manandhar S, Shutthanandan V, Ramana CV (2017) Controlled optical properties via chemical composition tuning in molybdenum-incorporated β-Ga_2O_3 nanocrystalline films. Chem Phys Lett 684:363–367

[17] Kumar SS, Rubio EJ, Noor-A-Alam M, Martinez G, Manandhar S, Shuthanandan V (2013) Structure, morphology, and optical properties of amorphous and nanocrystalline gallium oxide thin films. J Phys Chem C 117:4194–4200

[18] Tang X, Huang X, Huang Y, Gou Y, Pastore J, Yang Y, Xiong Y, Qian J, Brock JD, Lu J, Abruna HD, Zhuan L (2018) High-performance Ga_2O_3 anode for lithium ion batteries. ACS Appl Mater Interfaces 10:5519–5526

[19] Wang X, Zeng X, Cao D (2018) Biomass-derived nitrogen-doped porous carbons (NPC) and NPC/polyaniline composites as high performance supercapacitor materials. Eng Sci 1:55–63

[20] Du W, Wang X, Zhan J, Sun X, Kang L, Jiang F, Zhang X, Shao Q, Dong M, Liu H, Murugadoss V, Guo Z (2019) Biological cell template synthesis of nitrogen-doped porous hollow carbon spheres/MnO_2 composites for high-performance asymmetric supercapacitors. Electrochim Acta 296:907–915

[21] Idrees M, Batool S, Kong J, Zhuang Q, Liu H, Shao Q, Lu N, Feng Y, Wujcik EK, Gao Q, Ding T, Wei R, Guo Z (2019) Polyborosilazane derived ceramics-nitrogen sulfur dual doped graphene nanocomposite anode for enhanced lithium ion batteries. Electrochim Acta 296:925–937

[22] Qi H, Teng M, Liu M, Liu S, Li J, Ya H, Teng C, Huang Z, Liu H, Shao Q, Umar A, Ding T, Gao Q, Guo Z (2019) Biomass-derived nitrogen-doped carbon quantum dots: highly selective fluorescent probe for detecting Fe^{3+} ions and tetracyclines. J Colloid Interface Sci 539:332–341

[23] Deng W, Kang T, Liu H, Zhang J, Wang N, La N, Ma Y, Umar A, Guo Z (2018) Potassium hydroxide activated and nitrogen doped graphene with enhanced supercapacitive behavior. Sci Adv Mater 10:937–949

[24] Shindume L, Zhao Z, Wang N, Lu H, Umar A, Zhang J, Wu T, Guo Z (2019) Enhanced photocatalytic activity of B, N-codoped TiO_2 by a new molten nitrate process. J Nanosci Nanotechnol 19:839–849

[25] Huang J, Li Y, Cao Y, Peng F, Cao Y, Liu H, Guo Z (2018) Hexavalent chromium removal over magnetic carbon nanoadsorbents: synergistic effect of fluorine and nitrogen co-doping. J Mater Chem A 6:13062–13074

[26] Mayer M, SIMNRA (1999) A simulation program for the analysis of NRA, RBS and ERDA. In: AIP Conf. Proc. AIP, pp 541–544

[27] Ghosh SC, Biesinger MC, LaPierre RR, Kruse P (2007) X-ray photoelectron spectroscopic study of the formation of catalytic gold nanoparticles on ultraviolet-ozone oxidized GaAs(100) substrates. J Appl Phys 101:114322

[28] Naumkin AV, Kraut-Vass A, Gaarenstroom SW, Powell CJ (2012) NIST Standard Reference database 20

[29] Hollinger G, Skheyta-Kabbani R, Gendry M (1994) Oxides on GaAs and InAs surfaces: an x-ray-photoelectron-spectroscopy study of reference compounds and thin oxide layers. Phys Rev B 49:11159

[30] Syed N, Zavabeti A, Mohiuddin M, Zhang Y Wang, Datta RS, Atkin P, Carey J, Tan C, van Emdes J (2017) Sonication-assisted synthesis of gallium oxide suspensions featuring trap state absorption: test of photochemistry. Adv Funct Mater 27:1702295

[31] Ramana CV, Rubio E, Barraza C, Miranda Gallardo A, McPeak S, Kotru S, Grant J (2014) Chemical bonding, optical constants, and electrical resistivity of sputter-deposited gallium oxide thin films. Appl Phys 115:043508

[32] Trinchi A, Kaciulis S, Pandolfi L, Ghantasala MK, Li YX, Wlodarski W, Viticoli S, Comini E, Sberveglieri G (2004) Characterization of Ga_2O_3 based MRISiC hydrogen gas sensors. Sens Actuators B 103:129–135

[33] Ou S-L, Wuu D-S, Fu Y-C, Liu S-P, Horng R-H, Liu L, Feng Z-C (2012) Growth and etching characteristics of gallium oxide thin films by pulsed laser deposition. Mater Chem Phys 133:700–705

[34] Bharti B, Kumar S, Lee H-N, Kumar R (2016) Formation of oxygen vacancies and Ti^{3+} state in TiO2 thin film and enhanced optical properties by air plasma treatment. Sci Rep 6:32355

[35] Xu N, Liu L, Sun X, Liu X, Han D, Wang Y, Han R, Kang J, Yu B (2008) Characteristics and mechanism of conduction/set process in TiN/ZnO/Pt resistance switching random-access memories. Appl Phys Lett 92:232112

[36] Hussain H, Tocci G, Woolcot T, Torrelles X, Pang CL, Humphery DS, Yim CM, Grinter DC, Cabailh G, ikondoa O, Lindsay R, Zegenhang J, Michaelidas A, Thornton G (2016) Structure of a model TiO_2 photocatalytic interface. Nat Mater 16:461

[37] González-Elipe A, Munuera G, Espinos J, Sanz J (1989) Compositional changes induced by 3.5 keV Ar + ion bombardment in Ni-Ti oxide systems: a comparative study. Surf Sci 220:368–380

[38] Massaro CC, Rotolo P, De Riccardis F, Milella E, Napoli A, Wieland M, Textor M, Spencer N (2002) Comparative investigation of the surface properties of commercial titanium dental implants. Part I: chemical composition. J Mater Sci Mater Med 13:535–548

[39] Tao J, Luttrell T, Batzill M (2011) A two-dimensional phase of TiO_2 with a reduced bandgap. Nat Chem 3:296–300

[40] Gupta R, Sen S (1975) Calculation of multiplet structure of core p-vacancy levels II. Phys Rev B 12:15

[41] Leedy KD, Chabak KD, Vasilyev V, Look DC, Boeckl JJ, Brown JL, Tetlak SE, Green AJ (2017) Highly conductive homoepitaxial Si-doped Ga_2O_3 films on (010) β-Ga_2O_3 by pulsed laser deposition. Appl Phys Lett 111:012103

[42] Ramana CV, Baghmar G, Rubio EJ, Hernandez MJ (2013) Optical constants of amorphous, transparent titanium-doped tungsten oxide thin films. ACS Appl Mater Interfaces 5:4659–4666

[43] Kalidindi N, Manciu F, Ramana CV (2011) Crystal structure, phase, and electrical conductivity of nanocrystalline $W_{0.95}Ti_{0.05}O_3$ thin films. ACS Appl Mater Interfaces 3:863–868

[44] Geller S (1960) Crystal structure of -Ga_2O_3. J Chem Phys 33:676–684

[45] Egerton RF (2005) Physical principles of electron microscopy. Springer, Berlin

[46] Battu AK, Manandhar S, Ramana CV (2018) Nanomechanical characterization of titanium incorporated gallium oxide nanocrystalline thin films. Mater Today Nano 2:7–14